Instrument Science Report WFC3 2007-25

WFC3 TV2 Testing: IR Channel Non-linearity Correction and Unstable Pixel Masking

B. Hilbert
1 November 2007

ABSTRACT

Using data taken during WFC3's Thermal Vacuum 2 (TV2) testing campaign, we have characterized the non-linearity of the IR-1 detector. Cubic polynomials were used to fit the signal and produce correction coefficients to remove the non-linearity effects. We have also created a mask that identifies pixels with non-nominal behavior. This population of pixels represents 4.1% of the total number of active pixels in the IR channel, and should be ignored in subsequent data analyses. A minimum of 5.2% of the active pixels fail to meet the CEI Spec for a saturation level above 70,000 e^-.

Introduction

During TV1 testing in 2004, the non-linear behavior of IR-2 (FPA64) was characterized and reported in Robberto and Hilbert (2005). A new IR detector package has subsequently been installed in WFC3. The purpose of this work was to characterize the non-linearity of the new detector (FPA129) using similar methods to those described in Robberto and Hilbert. The ultimate goal was to create, using TV2 data, a method to correct the IR channel non-linearity in accordance with the appropriate CEI Specifications.

During this investigation, we also identified a population of pixels in the IR channel with non-nominal behavior. These pixels showed unpredictable, inconsistent

behavior from ramp to ramp under constant conditions. Several tests were designed to identify and mask these pixels, which would otherwise have a detrimental effect on various data analyses.

Data

Data ramps taken for this study were from the IR04S11 SMS. This SMS specified 10 SPARS10 flat field images, taken through F125W and illuminated by the CASTLE Tungsten lamp. Ideally, the illumination level would be enough to cause all of the pixels on the IR detector to go non-linear by >5% by the end of each ramp. This was not achieved in all pixels. 11% of the active pixels did not go non-linear to this level. For these cases, non-linearity corrections were derived, but the level at which they saturate are unknown. A repeat of this test in TV3 should use an increased incident flux level, in order to produce more accurate non-linearity corrections and saturation levels.

List of Observations

Exposure Type	*Number of Ramps*	*Sample Sequence*	*Reads per Ramp*
Dark	1	SPARS10	13
Flat field	10	SPARS10	13
Dark	1	SPARS10	13

Table 1: Datasets used for the non-linearity and unstable pixel investigation.

Prior to any data analysis, the ramps were run through the IDL data reduction pipeline (Hilbert, 2004), in order to subtract bias signal, pixel-to-pixel variations in reset voltage, and any cosmic rays that might have been present in the data. We also renormalized the signal in each pixel by subtracting the signal in the first read from all subsequent reads. To convert ADU to electrons, we used gain values of 2.42, 2.44, 2.41, and 2.46 e^-/ADU for quadrants 1 through 4, respectively. Gain calculations will be detailed in a subsequent ISR. We follow the convention established by Hartig (priv. communication) where quadrant 1 is the upper left quadrant of the detector, with quadrant numbers increasing counter-clockwise.

Analysis

Analyses of these data were broken down into two main steps. First, we identified and filtered pixels exhibiting unpredictable or inconsistent behavior. The locations of these pixels were saved as a mask to be applied to subsequent datasets taken with the current IR detector. Second, with the remaining good pixels, we parameterized

the non-linearity of the IR detector by fitting a cubic polynomial to the signal. These coefficients allow ramps taken with the current IR detector to be linearized.

Unstable Pixel Search

The search for unstable pixels was in itself a multi-step process. Examination of the ramps associated with this test revealed several different flavors of pixels with inconsistent behavior throughout the test. The specifics of these flavors are described in the list below, and examples are shown in Figures 1 and 9.

1. Pixels which show nominal behavior in most ramps, but an elevated signal rate in one or some ramps.
2. Pixels with initially consistent signal rates, but inconsistent behavior approaching saturation. The saturation rate in these pixels appeared to vary from ramp to ramp.
3. Pixels with consistent saturation levels, but slightly varying initial signal rates in the lower signal portion of the ramps

In Figure 1, the pixel exhibits unstable behavior. For 9 of the 10 data ramps, the pixel registers very low signal levels, with significant ramp-to-ramp variation. In the tenth ramp, the pixel measures a much larger signal, saturating in the 80,000 to 100,000 e^- range. The reason behind this instability is not understood. Given the unpredictable behavior of this pixel, it must be flagged as unusable.

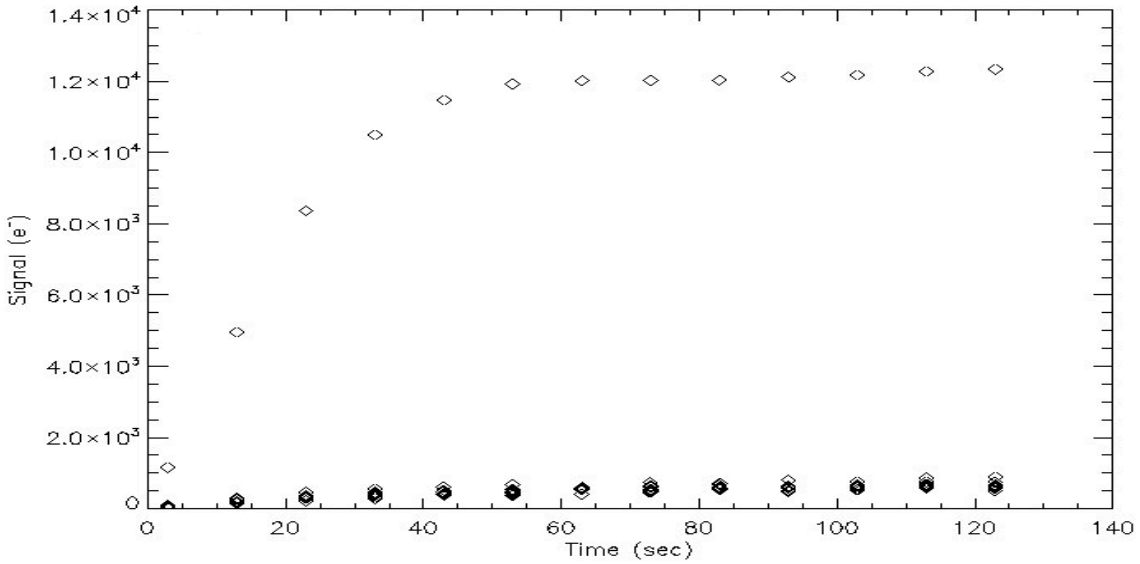

Figure 1: Signal measured by an unstable pixel for the 10 flat field ramps listed in Table 1.

As a first-cut search for these unstable pixels, we fit a line to the signal up the ramp in each pixel. This was repeated for all 10 ramps. We then used IDL's resistant_mean.pro and robust_sigma.pro to calculate the mean and standard deviation of the best-fit slope, best-fit intercept, and chi squared, for each pixel. Comparing the best fit parameters of each individual ramp to these mean values, we flagged pixels in which any of the three parameters were more than 5-sigma from their respective means. The thought behind this is that pixels which behave consistently except for one or two ramps out of 10 will easily be caught with this method. Pixels that might have consistent signal rates, but with widely varying saturation levels will also be caught. Setting the threshold for the three parameters at 5-sigma led to 4.1% of the active pixels being caught as bad.

Calculate Non-linearity Correction Coefficients

The second search for unstable or strange pixels was performed during the calculation of non-linearity correction coefficients and the saturation map. Coefficients were calculated in a manner very similar to that described by Robberto and Hibert (2005), with minor changes.

First, we created a median ramp using the 10 flat field ramps listed in Table 1. Pixels identified as unstable in the previous section were masked and ignored. For every good pixel, we fit a line to the signal in the first 2 reads of the median ramp. We are limited to only the first 2 reads because most of the pixels are immediately non-linear from the beginning of the ramp. As we wanted to examine the behavior of the residual signal after removing the ideal linear signal, a linear fit to more than the first two reads did not give a true representation of the ideal signal, and resulted in residuals that were not well fit by Equation 1. An attempt was made to identify alternate functional forms for these residuals, but was unsuccessful. Figure 1 shows a single ramp for one pixel, along with the best-fit linear signal.

Once the linear best-fit signals up the ramp were determined for a given pixel, we created ratios of the best-fit signal to the original signal, as seen in Figure 2.

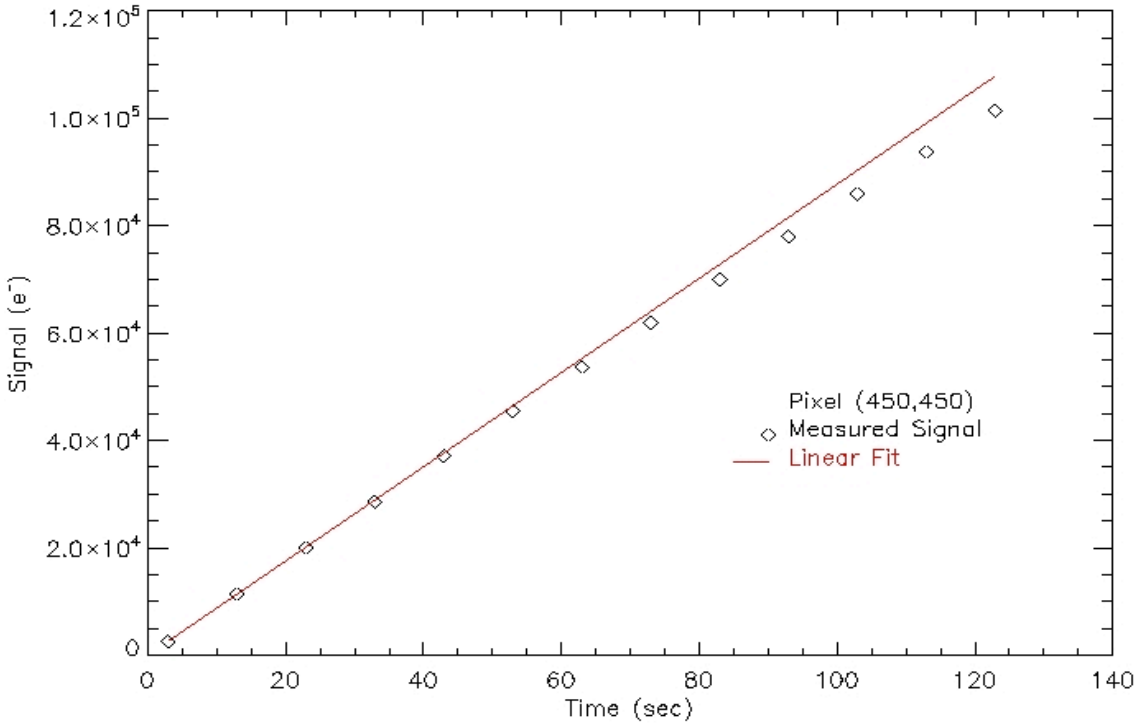

Figure 2: Measured signal for one pixel during one ramp, along with a linear fit to the first two reads.

The goal of the next step was to fit a function, shown in Equation 1, to these ratios. The motivation behind the use of this function is described in more detail in Robberto and Hilbert (2005). We modified the equation as it appears in that text by adding the constant and linear terms. These extra terms resulted in better fits to the ratio data from FPA129, due to the previously described low signal level non-linearity observed in some pixels. For fitting purposes we also subtracted 1.0 from the ratio values, such that exactly linear signals (ie identical measured signal and signal extrapolated from the linear fit) give a value of 0.

$$y = A + Bx + Cx^2 + Dx^3 \qquad 1)$$

In the end we wanted coefficients for Equation 1 for each stable, active pixel on the detector. Pixel-by-pixel, we fit Equation 1 to the ratio values from all 10 ramps for a

given pixel simultaneously. As seen in Figure 3 (which shows ratio values for only a single ramp of a single pixel), we fit the ratio data as a function of the original measured signal, as this is the quantity on which we will eventually be performing the non-linearity correction. For each pixel, we recorded the values of *A*, *B*, *C*, and *D*, as well as the reduced χ^2 for the fit.

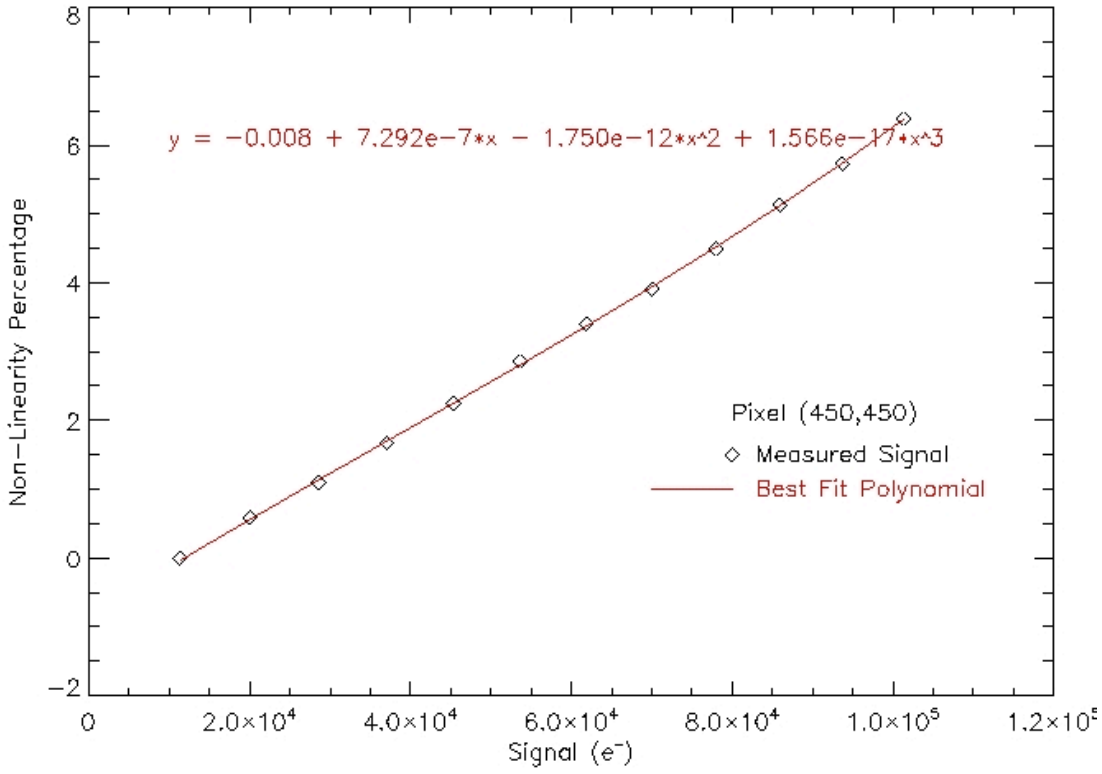

Figure 3: Ratio of best-fit line to the ramp versus the measured signal, along with the best-fit 3rd order polynomial.

Similar to the procedure used in the TV1 testing, we identified additional (roughly 2,000) pixels exhibiting strange behavior based on the χ^2 values from the curve fitting. Pixels with large χ^2 values displayed non-linear characteristics that did not fit the model well. This implied that a non-linearity correction based on Equation 1 would not adequately linearize the measured signal in these pixels. Following the convention established from the TV1 data, we flagged as bad any pixel with a value of the reduced χ^2 greater than 0.2. 0.3% of the active pixels fell into this category. Figure 4 shows a histogram of the χ^2 values for all pixels.

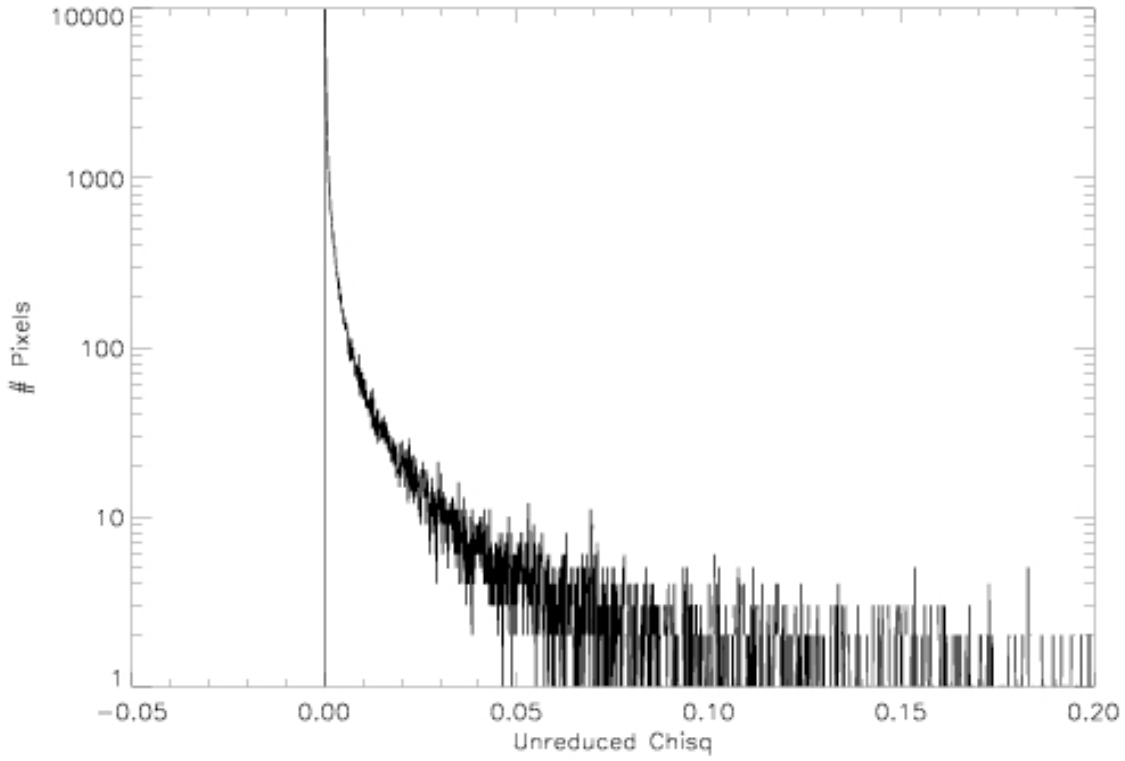

Figure 4: Log-scaled histogram of the X^2 values from the polynomial fit to the data ratios.

Figures 5 and 6 show plots of the *A* versus *B* values for all active pixels on the detector. Pixels meeting our χ^2 criteria are highlighted in red in Figure 5. Figure 6 shows the A and B values for only the pixels meeting the χ^2 criteria. Figures 7 and 8 show the same information, for values of C and D. As seen in TV1, the pixels that fit the model best all share a relatively narrow range of *C* and *D* values. A final mask of unstable and non-nominal pixels was created by combining this χ^2 mask with the mask created from the unstable pixel search outlined above. This final mask has 4.4% of the active pixels marked as bad.

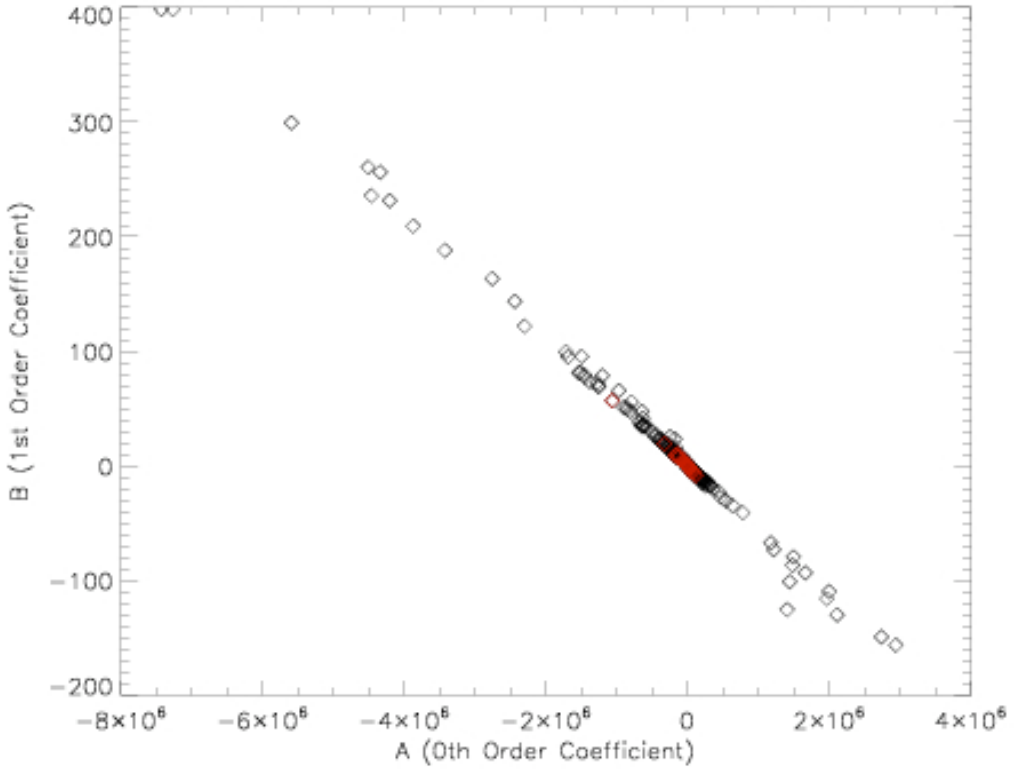

Figure 5: Best-fit A versus B values. Those in red indicate a stable pixel, while those in black are for pixels falling outside of the $\chi^2 < 0.2$ criteria.

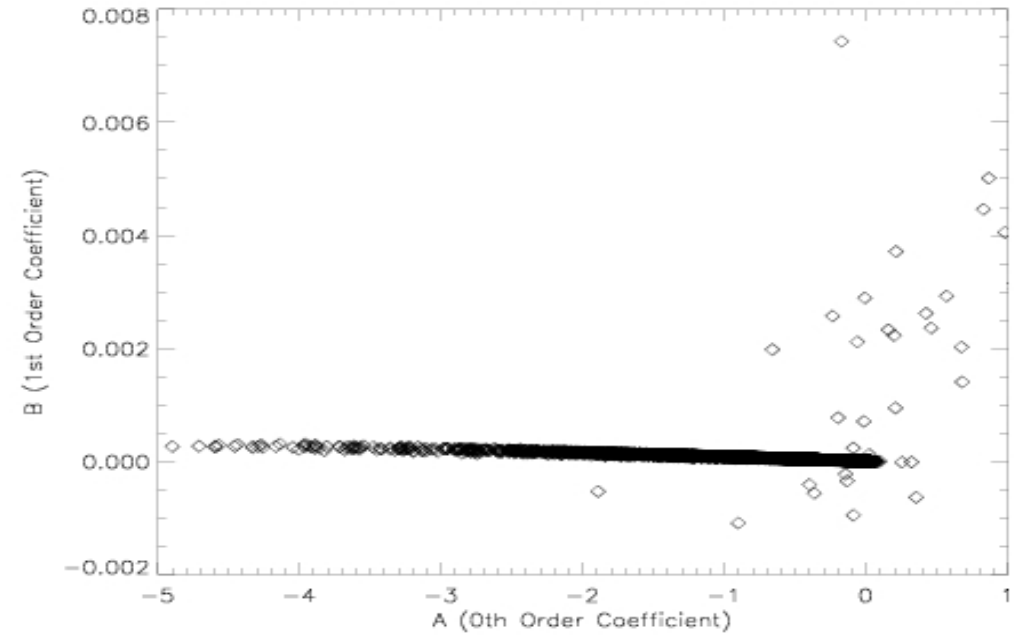

Figure 6: Best-fit A versus B Values for pixels with χ^2 less than 0.2.

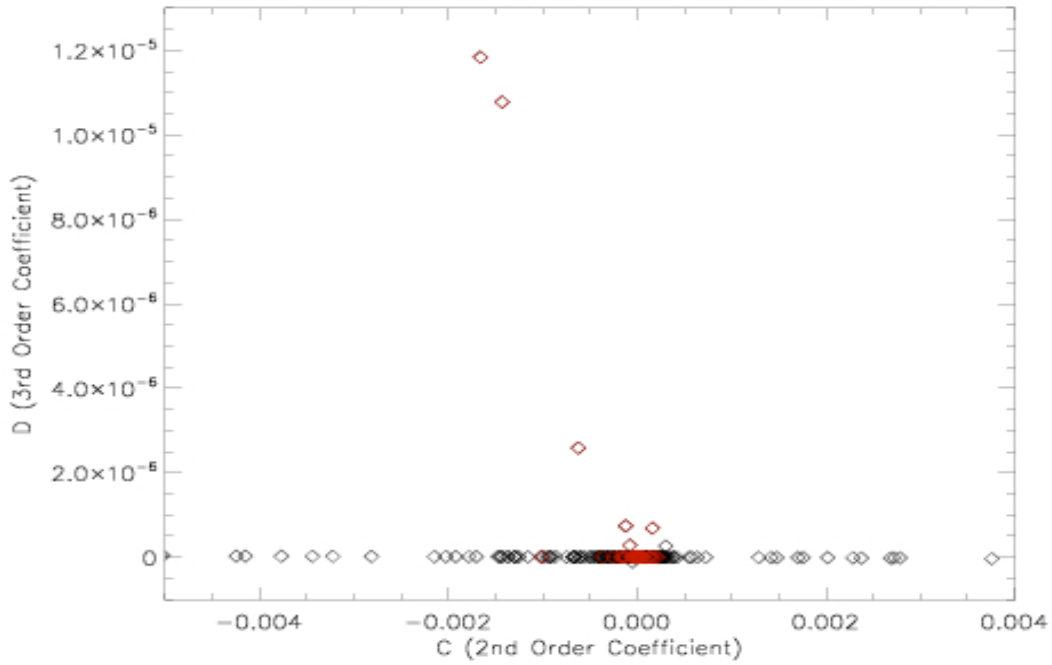

Figure 7: Same as Figure 4, but for best-fit values of C and D.

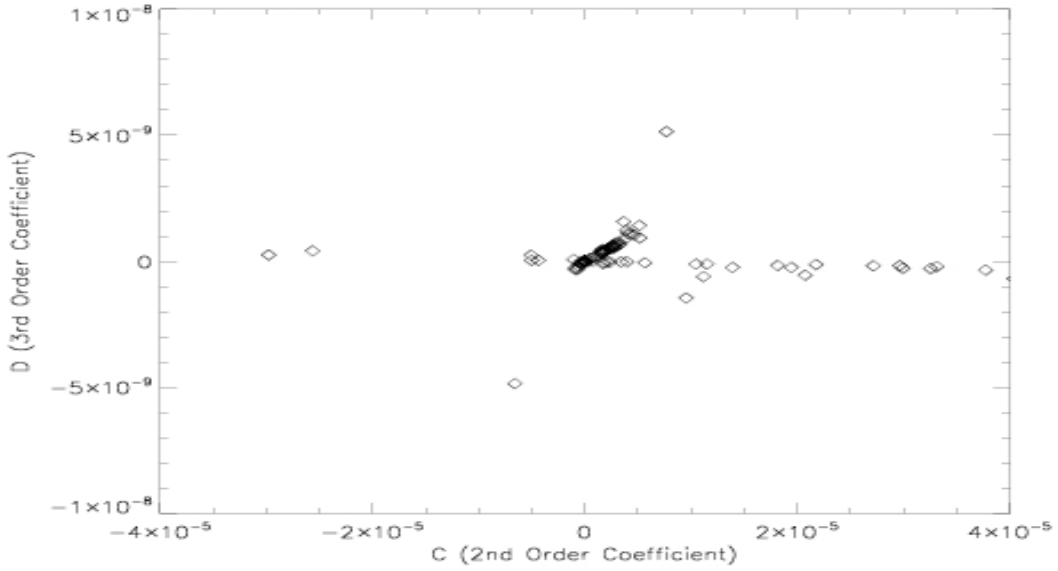

Figure 8: Best-fit C versus D values for pixels with χ^2 less than 0.2.

Figure 9 shows an example of a pixel that fails to meet the χ^2 criteria. This pixel shows unstable behavior across the 10 ramps in this study. The highly variable saturation level, as well as errors at lower signal levels that are much larger than Poisson uncertainties, means that accurate photometry with this pixel would not be possible.

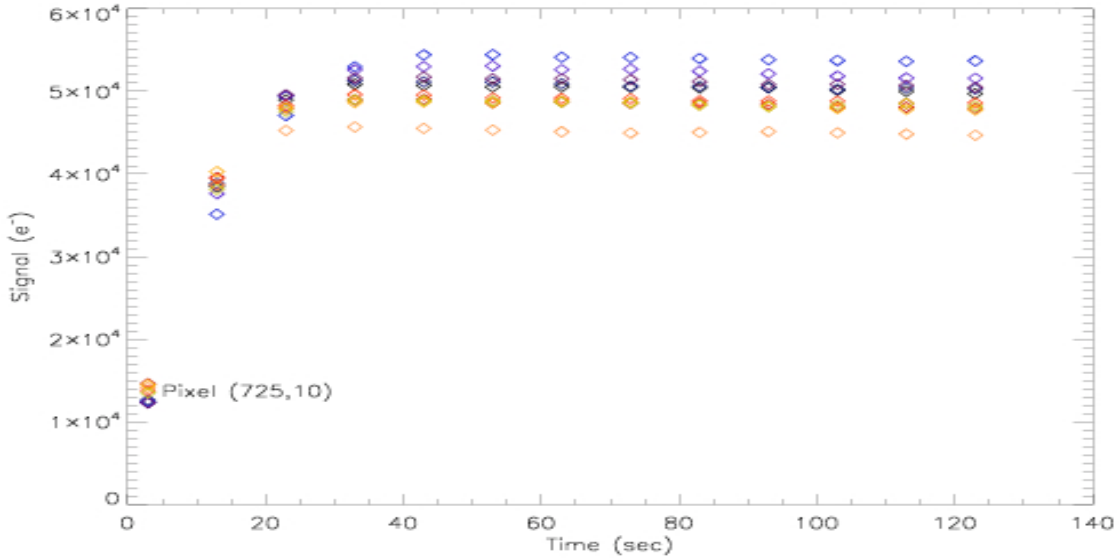

Figure 9: Signals measured in all 10 ramps for a pixel that fails to meet our χ^2 criteria.

After the calculation of the non-linearity correction coefficients, the final product needed for a full, generalized correction was a saturation map. CEIS 4.8.8 dictates that pixels in the IR detector must be linear to within 5%, and correctable to within 0.3%, for signals up to 70,000 electrons. Therefore, our desire was to create a saturation map that lists, for each pixel, the signal level at which that pixel becomes 5% non-linear. Above this level, the pixel is considered saturated, and the data are ignored.

Using the 10 ramps, with unstable, dead, and strange pixels masked, we created a median ramp. For the same reasons as stated in the initial linear fits, we calculated a best-fit line to the first two reads for each pixel. We then used least-squares quadratic interpolation to find the signal level where the original measured signal differed from the best-fit linear signal by 5%. This value was recorded as the pixel's saturation level. Masked pixels (4.1% of active pixels) were given IDL's NaN for saturation values. For the 2.3% of the active pixels that did not receive enough signal to ever go 5% non-linear, the saturation level was set to -99999. Further tests at higher illumination levels will be needed to calculate these saturation levels. Figure 10 shows a histogram of the calculated saturation levels. 88.5% of the active, unmasked pixels meet the CEI Spec, and have saturation levels at or above 70,000 e^-. This leaves 5.1% of the active pixels that have saturation levels below the CEI Spec level of 70,000 e^-.

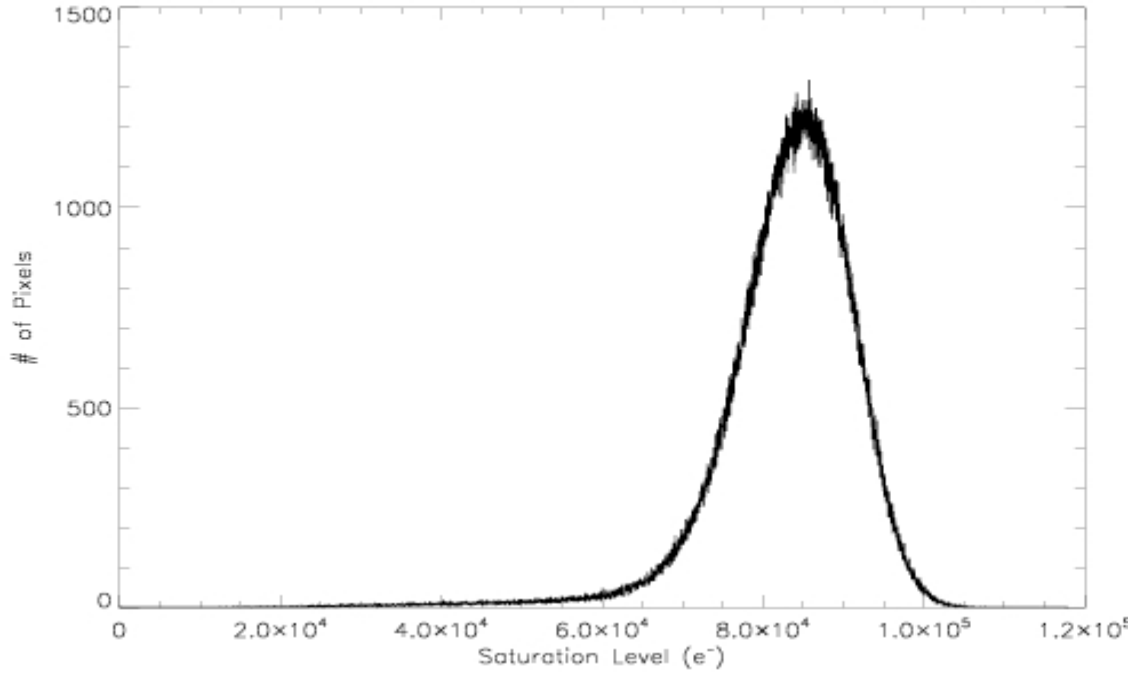

Figure 90: Histogram of the saturation levels for all unmasked active pixels. CEI Spec dictates a minimum saturation level of 70,000 e^-.

Upon completion of the saturation map, we saved the *A*, *B*, C, D, and saturation level values in a multi-extension FITS file. Using this file, along with the newly created IDL script ir_nonlinearity_correction.pro, any WFC3-IR ramp taken with FPA129 can have non-linearity effects removed, while bad pixels can be removed using the final mask file.

We tested the efficacy of these corrections in the ideal case. Using the ramps from which the coefficients were calculated, we applied the non-linearity correction and bad pixel mask. We linearized the signal in the original ramps, using our calculated coefficients and Equation 2, where *x* is the measured signal, and *y* is the corresponding linearized signal.

$$y = x * (1 + A + Bx + Cx^2 + Dx^3) \qquad 2)$$

After performing the correction on the 10 ramps used in this study, we calculated the difference between the corrected signal and an ideal signal, again made from a linear fit to reads 1 and 2 of the corrected data. CEIS 4.8.8 declares that the corrected signal should linear to better than 0.3% for all signal levels up to 70,000 electrons. Figure 11 shows the signal rate up the ramp for a single pixel in each of the 10 ramps both before and after the application of the non-linearity correction. Figure 12 shows the residual non-linearity in the same pixel, after the correction was performed, for each of the 10 ramps. At signal levels above 65,000 e-, this pixel is corrected to better than the CEI Spec level of 0.3%. Above 20,000 e-, the pixel reaches a non-linearity of no more than 0.7%, matching the level of Poisson noise for this signal. For low signal levels, the residual non-linearity increases to as much as 2%. The effects of Poisson noise are shown in Figure 11 by the blue error bars. These errors are for the ramp that is shown as blue diamonds, and are the same length for all ramps. Once the effects of this Poisson noise is considered, we see that the corrected ramps have residual non-linearities within the specification of 0.3%.

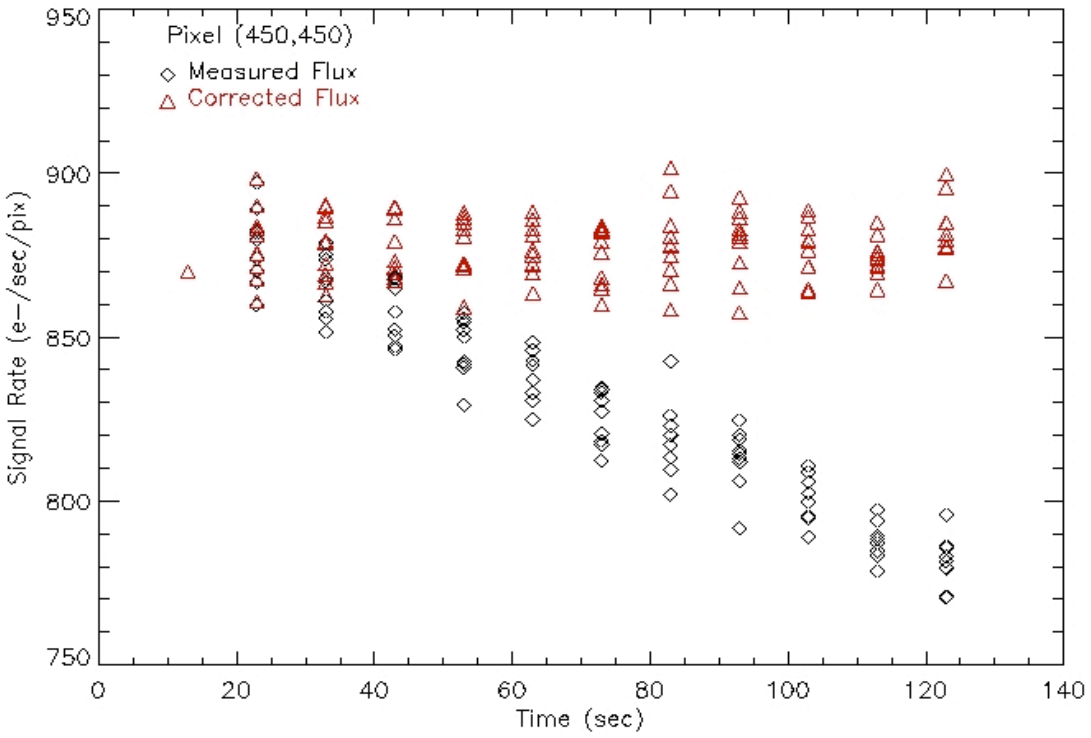

Figure 11: Measured signal rates in pixel (450,450) for all 10 ramps both before (black) and after (red) non-linearity correction.

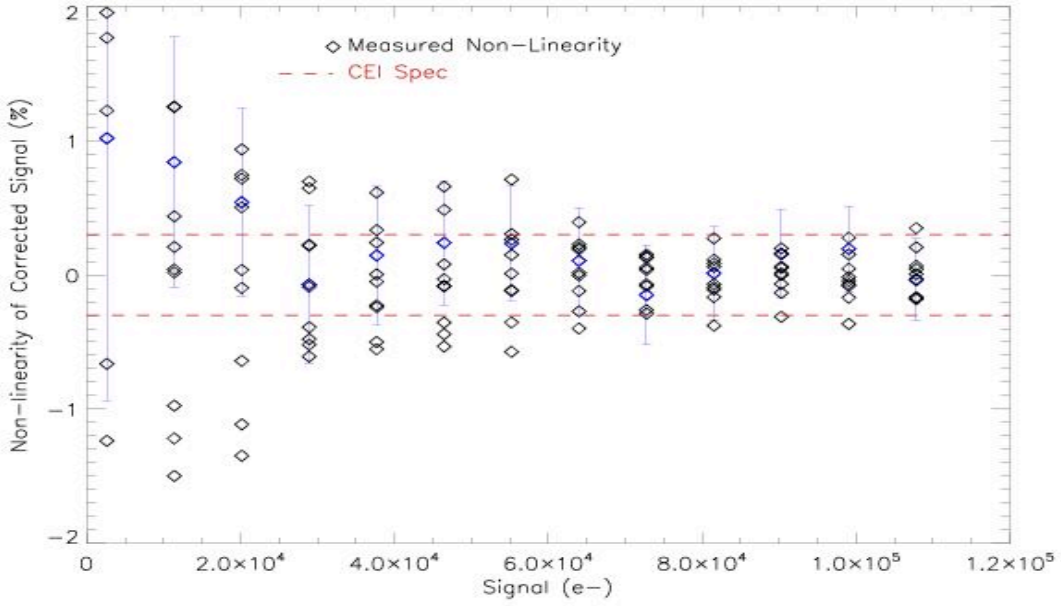

Figure 12: Residual non-linearity for pixel (450,450) in all 10 ramps, after the non-linearity correction has been applied. CEI Spec calls for a corrected non-linearity of no more than 0.3% for signals less than 70,000 e^-. After accounting for uncertainties due to Poisson noise (shown as blue error bars for one of the 10 ramps), we see that the non-linearity correction produces signals within the 0.3% specification.

Figure 13 examines the results of the non-linearity fix for an entire quadrant of the detector, rather than for a single pixel. This figure shows histograms of the residual non-linearity in all unmasked quadrant 4 pixels. Each histogram reveals the non-linearity at a different read in the corrected ramps. Consistent with the trend seen in Figure 12, the broad histograms with the largest non-linearities show the behavior in early, low-signal to noise reads, while the more strongly-peaked histograms are for later, higher-signal reads. The percentage of quadrant 4 pixels falling outside the CEI Spec of 0.3% post-correction non-linearity decreases with increasing read number from 50% down to 9% for this set of 10 ramps. Throughout this study, non-linearity has been defined as the ideal, linear signal minus the measured signal. This definition leads to positive values of non-linearity in the original IR channel ramps. The fact that the measured residual non-linearities in Figures 12 and 13 are centered around 0, rather than all positive, suggests that the intrinsic ramp-to-ramp variation (ie Poisson noise) in measured signal is the cause of the residual non-linearity.

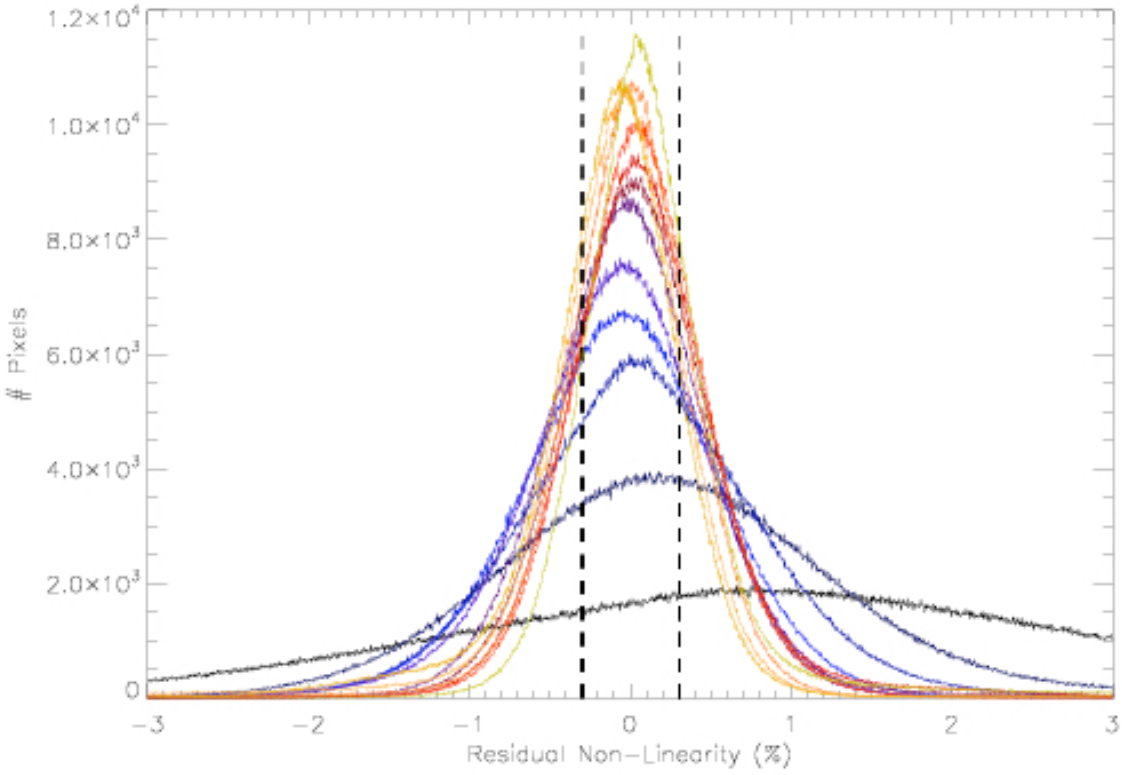

Figure 13: Histograms of residual non-linearity for quadrant 4 of the IR detector. Each histogram represents one read of the detector across all 10 ramps. For example, the shortest and widest histogram shows the non-linearity in read 1 of all 10 ramps. As the read number (and signal) increases, the histograms become more narrow and strongly peaked.

Conclusions

Using the set of 10 flat field ramps taking during TV2 testing, we find that a minimum of 5.1% of the total active pixels fail to meet the CEI Spec for saturation level. An additional 2.3% of the active pixels must measure higher signal levels in order to calculate saturation values.

From this set of 10 ramps, we have created a set of non-linearity correction coefficients capable of removing most of the non-linear effects from FPA129. Using this well-tested method, we will be able to quickly calculate a non-linearity correction for the IR detector to be used in TV3 testing.

Recommendations

This test will be repeated in TV3 testing, scheduled for early 2008. The flux levels provided by CASTLE should be increased for that test, in order to ensure that all pixels reach saturation.

References

Hilbert, B. ***Basic IDL Data Reduction Algorithm for WFC3 IR and UVIS Channel.*** WFC3 ISR 2004-10. http://www.stsci.edu/hst/wfc3/documents/ISRs/WFC3-2004-10.pdf 10 June 2004.

Robberto, M. and B. Hilbert. ***WFC3 2004 Thermal Vacuum Campaign: IR channel linearity (flat field illumination - SMS IR04).*** WFC3 ISR 2005-29. http://www.stsci.edu/hst/wfc3/documents/ISRs/WFC3-2005-29.pdf 7 Dec 2005.